

Modeling Attenuation of Storm Surge over Deformable Vegetation: Methodology and Verification

Minati Mohanty, Papun Kumar Rout,

Gandhi Institute of Excellent Technocrats, Bhubaneswar

KMBB College of Engineering and Technology, Khordha, Odisha, India

ABSTRACT: This study extended and unified resistance formulations for rigid and deformable plants under both the emergent and submerged conditions. Three approaches were examined in detail and implemented into a numerical model. First, the flow resistance formulations for rigid plants were critically reviewed. By introducing plant deformation relations with a given vegetal stress and vegetation properties, the formulation for rigid plants was extended to flexural rigid plants. Second, a flow resistance formulation directly derived from submerged, flexible plants was examined and extended. Both approaches to simulating deformable vegetations solve a set of two equations, a vegetation deformation relation and a resistance law, iteratively. The methodology and numerical algorithm for rigid and deformable plants were implemented into an operational storm surge model and tested against laboratory data. Good agreement has been found. The verified model can be used to study the spatial and temporal variations of deflected vegetation heights and equivalent Manning's coefficient under realistic hurricane and wetland conditions.

Author keywords: Storm surge; Wetlands; Vegetation; Flow resistance; Numerical modeling.

I. INTRODUCTION

Coastal wetlands play an important role in protecting coastal communities and stabilizing shorelines (Costanza et al. 2008; Gedan et al. 2011; Shepard et al. 2011). It is commonly accepted that vegetation can attenuate not only short waves (e.g., Mendez et al. 1999; Chen and Zhao 2012; Jadhav et al. 2013) but also long waves such as tsunami waves. For instance, it was observed that mangrove swamps effectively attenuated tsunami waves and protected a sheltered community while communities without the protection of mangroves were damaged severely (Latief and Hadi 2007; Alongi 2008; Teo et al. 2009). However, whether coastal wetlands can effectively attenuate forced long waves such as storm surges remains under debate (Resio and Westerink 2008; Feagin et al. 2010). Since Hurricane Katrina struck New Orleans, Louisiana, in 2005, more attention has been drawn to the potential benefits of coastal wetlands for reducing storm surge. Field measurements and numerical simulations in recent years are in support of vegetation's role in storm surge reduction (e.g., Loder et al. 2009; Wamsley et al. 2009; Shen et al. 2012). Wetland restoration is advocated from both the ecological and flood-reduction perspectives (Walton et al. 2006; Day et al. 2007). Typically, surface waves that may cause damages to coastal communities include short waves (wind- or boat-generated), tsunamis, and storm surges. Short waves are generated by winds or moving boats with wave periods of sec-

onds. Tsunamis often result from seismic

¹Coastal Hydrologist, ARCADIS-US, 10352 Plaza Americana

Dr., Baton Rouge, LA 70816; formerly, Postdoctoral Researcher, Dept. of Civil and Environmental Engineering, Louisiana State Univ., Baton Rouge, LA 70803 (corresponding author). E-mail: haihong.zhao@arcadis-us.com

²Professor, Dept. of Civil and Environmental Engineering and Center for Computation and Technology, Louisiana State Univ., Baton Rouge, LA 70803.

Note. This manuscript was submitted on August 16, 2012; approved on September 3, 2013; published online on September 5, 2013. Discussion period open until October 2, 2014; separate discussions must be submitted for individual papers. This paper is part of the Journal of Engineering Mechanics, ©ASCE, ISSN 0733-9399/04014090(11)/\$25.00.

activity or landslides on the ocean floor, and consist of a series of waves with the period ranging from minutes to hours. Storm surges as a gradual rise of water lasting from hours to days are built up as a result of a combination of wind setup, low atmospheric pressure, wave setup, and interaction with tidal conditions. Tropical cyclones and extra-tropical storms produce storm surges with surge heights ranging 1–9 m depending on the wind intensity, the size of the storm, proximity to the landfall location, as well as local bathymetry and geometry (e.g., Chen et al. 2008). Small strips of coastal wetlands and forests that effectively attenuate wind waves and tsunami waves are typically insufficient for reducing storm surge. Potential benefits of coastal wetlands for reducing storm surge heights depend on the wetland size and vegetation properties. With the urgent need of coastal restoration and hurricane protection along the Louisiana coast, a number of science-based programs have been launched to sustain a coastal ecosystem that provides support and protection to the environmental economy of southern Louisiana and beyond [Louisiana Coastal Area Science & Technology Program (LCASTO) 2010; Louisiana Applied Coastal Engineering and Science Division (LACES) 2012; Louisiana Coastal Protection and Restoration Authority (CPRA) 2012]. Both numerical models and field measurements are primary tools to investigate the role of coastal wetlands in storm surge and wave reduction. Numerical simulations using increased bottom friction resulting from vegetation have shown that coastal wetlands together with other landscape features are able to attenuate storm surge and waves to some extent (Suhayda 1997; Loder et al. 2009; Wamsley et al. 2009, 2010). The dominant vegetative resistance to the flow in various circulation or storm surge models is parameterized as an analog of the bottom friction using an enhanced, static Manning's coefficient (n), which may not be adequately accurate according to recent studies (e.g., Kouwen and Li 1980; Wu et al. 1999; Freeman et al. 2000; Wilson and Horritt 2002; Carollo et al. 2005; Wilson 2007). Vegetation-induced drag force, as an extra force exerted on the flow, was originally explored in the literature primarily for determining the discharge capacity of an open channel with submerged or emergent vegetation. For a given energy slope, the vegetative flow resistance becomes dominant as vegetation density increases. Lopez and Garcia (1998) showed that the bed shear stress of a vegetation field, with a 0.3 ratio of the stem frontal area to the substrate area where the stems shoot and are rooted, is only 20% of the value experienced by a bare bed. The diminished bed shear stress entrains fewer bottom sediments (Lopez and Garcia 1998) because the rooting soil has been strengthened

physically and biologically by vegetation (Micheli and Kirchner 2002). Therefore, the bed stress resulting from the bottom friction is often neglected (Fenzl and Davis 1964; Carollo et al. 2005). The drag force caused by vegetation is composed of the form drag, inertial force, and skin friction, while the latter two are often neglected in a time-averaged model. Therefore, the vegetation-induced drag force is simply considered as the form drag.

The vegetative drag force is commonly computed using the quadratic friction law, where the hydraulic relationship is utilized to determine the flow resistance coefficient given a value of the Manning's roughness coefficient, n , and a hydraulic radius (Chow 1959). This relationship is widely adopted for floodplains, coastal plains, and other aquatic environments with the hydraulic radius replaced by a flow depth (e.g., Guardo and Tomassello 1995; Copeland 2000; Kouwen and Fathi-Maghadam 2000; Doncker et al. 2009; Buna et al. 2010; Dietrich et al. 2011). A reliable estimation of n -values for a given type of vegetation is critical for investigating the hydrodynamics and ecology of a wetland environment (Lee et al. 2000, 2004; Schaffranek 2004). The USGS had a guide for selecting n -values (Arcement and Schneider 1989) and suggested adding a constant to a base value for a channel bottom with a certain type of growing plants in addition to other adjustments resulting from the channel irregularity, variation of cross section area, and so on. Nevertheless, it was also stated that the effects of vegetation on n depend on the flow depth, the population density of vegetation, the degree to which the vegetation is flattened by strong currents, and the alignment of vegetation relative to the flow. As those influencing factors were identified, various laboratory experiments and field measurements have been undertaken to quantify the relationships with n . Manning's n was found to vary seasonally as a result of the seasonal variation of vegetation biomechanical properties and above-ground biomass (e.g., Shih and Rahi 1982; Doncker et al. 2009). More importantly, n varies with the flow stage. Typically, as water depth increases, n increases for emergent plants and decreases for submerged plants (Wu et al. 1999; Wilson and Horritt 2002; Wilson 2007). When considering the flexibility of vegetation, n decreases as the flow velocity increases because a fast flow would bend the flexible vegetation and reduce the effective roughness height (Kouwen and Fathi-Maghadam 2000; Lee et al. 2000). The variation of n with the

flow depth and flow velocity leads to a re-relationship between n and the product of flow velocity and flow depth proposed in Palmer (1945) and denoted as the n -VR curve. However, because of the large discrepancy in n -VR curves (e.g., Kouwen and Li 1980; Wilson and Horritt 2002; Carollo et al. 2005), this re-relationship is physically meaningful yet not practical owing to the absence of the vegetation biomechanical properties. On the other hand, a drag coefficient is often used, especially when the underlying physics of flow-vegetation interaction are concerned. A large number of laboratory experiments have been performed to investigate the drag coefficient of an individual plant shoot within a group of the same kind and the corresponding drag force resulting from both rigid and flexible vegetation (live or artificial) under either emergent or submerged conditions (e.g., Tsujimoto et al. 1996; Lopez and Garcia 1997; Nepf 1999; Stone and Shen 2002; Wilson et al. 2003). Note that drag coefficients were defined with respect to different reference flow velocities. In addition to the well-known drag coefficient of an infinitely long isolated circular cylinder, a stem layer drag coefficient was introduced in Stone and Shen (2002) with respect to a spatially averaged velocity within the stem layer; a bulk drag coefficient was introduced in Nepf (1999) with a pore velocity averaged over the entire water column for a flow through an emergent canopy field; and a bulk drag coefficient with respect to the depth-averaged discharge velocity is useful for horizontal two-dimensional (2D) models. These drag coefficients are different in their reference velocities but similarly represent an array of rigid circular cylinders, where the flow is affected by adjacent cylinders. Nepf (1999) conducted a series of experiments in a flume covered with emergent cylinders. A dimensionless parameter of population density was used to represent the volume concentration of emergent stems. It was found that the bulk drag coefficient decreases as the population density increases for a stem Reynolds number (R_d) larger than 200. The reduction of the drag coefficient is caused by the velocity reduction in the affected wake structure and by the delayed point of separation at the downstream stem resulting from the upstream wake induced turbulence (Nepf 2004). However, the sheltering effect of the upstream cylinders on downstream elements are less significant for a lower stem density. Experimental data showed that the bulk drag coefficient remains nearly constant up to a population density of 0.01 (Nepf 1999) and the bulk drag coefficient can be approximated from that of a single cylinder (Stone and Shen 2002; Nepf 2004). The drag coefficient of a single cylinder depends on the stem Reynolds number, R_d , f

oralaminar regime, and is virtually equal to 1 up to $R_d \approx 533 \times 10^5$ (Naot et al. 1996; Nepf 2004; Wilson et al. 2006; Zhan et al. 2010). Stone and Shen (2002) conducted an extensive set of flume experiments on flow through both emergent and submerged rigid cylinders and showed that the drag coefficient of a single cylinder equals 1.05 with a small standard deviation for a wide range of population density, stem diameter, and R_d . The drag for a submerged, flexible canopy field is likely to be overestimated if plants are assumed to be rigid (Wilson and Horritt 2002), because a lower drag is expected as a result of the bending and streamlining of deformable plants. In reality, flexible plants are common, although they may act like rigid cylinders under flow conditions. A stiffness parameter, EI , which is the product of the modulus of elasticity and the second moment of the stem cross-section, was introduced as a measure of the plant flexibility and can be related to the deflected vegetation height and flow resistance (Kouwen and Unny 1973; Kouwen and Li 1980; Tsujimoto et al. 1996) for submerged plants. Fathi-Maghadam and Kouwen (1997) presented more evidence showing the reduction of the flow resistance resulting from vegetation flexibility under emergent conditions. Wilson et al. (2003, 2006) emphasized the importance of vegetation deformation in determining the mean velocity of flow through submerged vegetation. In addition to plant flexibility, the degree of submergence is another key parameter that has a closer relation with the vegetation drag force, especially during a hurricane event when the total water depth changes with the rising and falling surge water level at different stages of the event. Submergence is defined as the ratio of flow depth to the vegetation height. The flow through a canopy field can be classified as emergent, submerged, and deeply submerged, as the dominant driving forces of the canopy flow vary with the submergence (Nepf 2004). The flow over a deeply submerged canopy consists of three layers including a logarithmic velocity profile up to the water surface, a stem flow layer inside the canopy, and a mixing layer in between. The logarithmic layer becomes dominant as the submergence increases (> 10) and the deeply submerged flow eventually resembles the unconfined flow (Nepf 2004). As the submergence decreases, the logarithmic layer becomes less important while the mixing layer persists. When the submergence decreases below 1.5 , the mixing layer takes up the nonvegetation layer up to the water surface (Nepf and Vivoni 2000) until the plants are

emergent with the water column occupied simply by the canopy. With different degrees of submergence, the drag force varies. The dependencies of the vegetative flow resistance on vegetation properties, flow depth, flow velocity, and the combination have been widely revealed in laboratory scale experiments, yet less recognized in numerical modeling. A vegetative flow resistance module considering these dependencies is desirable for a horizontal 2D storm surge model to (1) take into account effects of vegetation on storm surge reduction by wetlands, (2) quantify the flood risk reduction benefits, and (3) provide guidance for restoration project design. The purpose of this study is threefold: (1) to review different flow resistance relationships resulting from rigid and flexible vegetation; (2) to extend the existing formula to account for both the rigidity of vegetation and varying degrees of submergence; and (3) to develop a vegetation-surge dynamically coupled model for predicting the effect of vegetation on the mean flow, surge levels, and wind waves. The results from the study are presented in this paper. A future paper will document the study using simplified field conditions and hurricane forcing, which reveals the spatial and temporal variability of the equivalent Manning's coefficient in coastal wetlands during a hurricane and provides insight into surge-vegetation-wave interactions.

The paper is organized as follows. After the introduction, the "Methodology" section reviews the flow resistance laws proposed by Stone and Shen (2002) and Kouwen and Unny (1973), and integrates them for a full range of submergence and a variety of vegetation rigidity. Next, the integrated formulations are implemented into a storm surge model and the numerical algorithm is explained. Then the vegetative flow resistance module is tested against three sets of laboratory experimental data for emergent vegetation, submerged rigid vegetation, and submerged deformable vegetation. The findings are summarized in the "Summary and Conclusions" section.

where τ_v is vegetative stress; C_D is bulk drag coefficient with bulk drag coefficient C_p can be related to the C_D under emergent conditions ($H^w \geq h$) by applying the corresponding velocity. Considerable efforts have been made in the literature to understand the flow structure and turbulence characteristics in deeply submerged

This paper is focused on model development and verification using laboratory vegetative flow resistance, either a drag coefficient or an equivalent Manning's coefficient needs to be determined. Both coefficients can be related to a dimensionless friction factor that is commonly used in the quadratic law [Eq. (1)]

$$\tau_v = \frac{1}{2} r_w f_v V^2 \quad (1)$$

where τ_v is vegetative stress; r_w is water density; f_v is vegetative friction factor; and V is depth-averaged velocity (discharge over the gross cross-sectional area).

The drag coefficient of a single rod within an array varies as

a result of the upstream wake structure and vortex shedding (Nepf 1999; Barkdoll et al. 2004). Therefore, a drag coefficient representing the array is defined as a bulk drag coefficient and the vegetative stress is expressed based on the Morrison-type equation

$$\tau_v = \frac{1}{2} r_w C_D N B_v H^w V^2 \quad (2)$$

where C_D is

drag coefficient

reference velocity, \bar{V} is number of stems per square meter,

known as the stem density ($N = 1/d^2$); d is average rooting area of a single rod; d is average distance between two adjacent stems; B_v is stem diameter; and H^w is wetted vertical stem height that is equal to the water depth for emergent conditions or equal to the vegetation height for submerged conditions. Fig. 1 illustrates an array of cylinder rods and corresponding parameters. Table 1 lists reference velocities and the corresponding bulk drag coefficients.

It was found by Stone and Shen (2002) that if the maximum

depth-averaged velocity at a constricted section in the stem layer (V_c) is used, the drag coefficient C_D approximates the value of a single cylinder, which is nearly constant with a relative standard deviation of 7.6% for a wider range of experimental conditions. In Table 1, the

drag coefficient C_D is a function of the relative velocity V_c and V_c in Eq. (2). The relationship is expressed as

$$C_D = \frac{12 N B_v^2}{V_c} \quad (3)$$

where N is stem density and B_v is stem diameter. Emergent and submerged vegetation canopies (e.g., Shiel et al. 1995; Lopez

$$C_D^{1/4} C_D$$

and Garcia 1997; Nepf 1999; Järvelä 2005; Ghisalberti and Nepf 2006). However, a low-submergence flow (submergence is larger than but close to 1) with a turbulence mixing layer extended to the surface of the water column is less studied. During a hurricane, the vegetation experiences conditions that are emergent (submergence

D_p is less than one), near emergent (submergence is close to 1), and submerged (submergence is larger than one) as the storm surge water intrudes and retreats. The near emergent stage may be critical for understanding not only the surge reduction but also the vegetation mortality as the drag force is significant under near emergent conditions (Nepf and Vivoni 2000; Nikora et al. 2001). In this study, flow resistance formulations within a wide range of submergence are critically reviewed, extended, and integrated into a new algorithm to model the vegetative flow resistance for both rigid and

$$1 \quad 2B_v P_{III}^2$$

(3) In Nepf (1999), a population density was defined as NB^2 . Given a population density smaller than 0.01, C_D varies around 1.2 and is less affected by the population density. However, if the population density becomes large, C_D decreases as the effects of wake structure become significant. Consequently, C_D decreases as well. Applying

deformable plants. A notation table is provided for all symbols used in the text.

Rigid Cylinder Formulation

Formulations for rigid cylinders are discussed first because not only is understanding the flow resistance of rigid, cylindrical rods in a channel fundamental for studies on flexible plants, but also Eq. (3) and the population density of 0.01 yields $C_D 51:2$ $1C_D$. Thus, the authors have $C_D 51:2$ by assuming $C_D 51:0$ for sparse

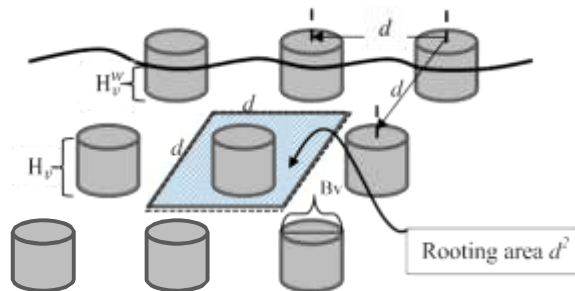


Fig.1. Schematic array of emergent flexible plants may act like rigid cylinders. To quantify

where P^5 ratio of the wetted stem height to the flow depth ($H^w = h$). Replacing (\check{V}, \check{C}_D) in Eq. (2) with (\check{V}, C_D) and (V_c, C_D^v) , respectively, and invoking Eq. (4) yields

$$h^P$$

The dependence of the friction factor on the submergence offers a way to determine the surge-dependent drag force. Nikora et al. (2001) studied the flow over a rough permeable or impermeable bed and showed three flow types with high submergence, ne

$$f_v^{1/4} \frac{C_D N B_v H_v}{1}, \text{ submergeds. } 1; H^w \approx 4 H_v \quad (7b)$$

$$\frac{C_D^{1/4} C_D}{2h^2 P B_v} \frac{P^{1111}}{N^2} \quad (5)$$

and relatively small submergence. They found that the Darcy-Weisbach friction coefficient [one-fourth of the friction factor in Eqs. (1), (6), and (7)] increases as the degree of submergence (s)

Eq. (5) suggests that the bulk drag coefficient, C_D , is positively related to the stem density, the stem diameter, and the vegetation height, and is inversely affected by the water depth for a given C_D . If the population density increases remarkably, C_D itself will reduce, and so will C_D , as a result of the effects of enhanced wake structure and vortex shedding with a high Reynolds number.

By combining Eqs. (1), (2), and (5), the vegetal friction factor can be expressed as increases for the emergent condition ($s = 1$), and then decreases as the submergence approaches 1 and continues to increase ($s < 1$).

Because Manning's coefficient is widely used in operational numerical models, it is worth noting that an equivalent Manning's coefficient (n_e) can be derived by employing the hydraulic relationship between the Manning's coefficient and the friction factor for uniform flow [$n_e 5 f_v = 2g^{1/2} h^{1/6}$]. Eq. (8) defines n_e as a function of the flow depth and various vegetation properties

$$\frac{C_D N B_v H^w}{12} \frac{H^w}{h} \frac{P^{1111}}{N^2} \quad (6)$$

$$n_e^{1/4} \frac{D}{v} \frac{v}{v} \frac{P^{1111}}{N} \quad (8)$$

Eq. (6) can be rewritten for the emergent and submerged conditions where g is acceleration due to gravity and all other symbols were defined in previous equations.

$$C_D N B_v H_v \frac{P^{1111}}{12 B_v N^2}$$

$$s, \text{ emergent } \#1; H^w \approx 4h \quad (7a)$$

It is observed from Eq. (8) that n_e increases as the population density and vegetation height increase, which is consistent with previous studies (e.g., Lopez and Garcia 2001; Wu 2008). For given

$$12 B_v \frac{P^{1111}}{N^2} s$$

where H_v is erect vegetation stem height; and s is degree of submergence defined as $s = h/H_v$. Therefore, the vegetal friction factor becomes a function of submergence in addition to vegetation properties.

Fixing all parameters but the submergence, the vegetal friction factor increases with s when $s < 1$, and then decreases as the submergence increases when $s = 1$, as shown by the solid curve in Fig. 2.

vegetation properties, n_e would increase as the water depth increases for emergent vegetation, which has been observed in laboratory studies (e.g., Wu 2008). When the vegetation is submerged and the water depth is sufficiently large ($s \rightarrow 1$), n_e approaches a constant. Note that the equivalent Manning's coefficient in Eq. (8) is not

a function of the flow velocity, which contradicts the VR curves in

previous studies of flexible vegetation (e.g., Wilson and Horritt 2002; Carollo et al. 2005). This is because the derivation is based on relationships for rigid cylinders. Rigid plants do not adjust themselves to the flow and result in drag coefficients independent of varying velocities for large Reynolds numbers. When the plant flexibility is considered, H^w is expected to change with the velocity, which is also the case for n_e . It has been documented that either the bulk drag coefficient or the equivalent Manning's coefficient reduces as the flow velocity increases (Freeman et al. 2000; Kouwen

and Fathi-Maghadam 2000). The next section provides a detailed discussion on deformable plants.

Extended Formulation for Deformable Plants

Natural grasses are flexible and adjust themselves to a water flow. Fig.3 illustrates a flexible plant bent by the drag force and notes the vegetation dimensions. Because of the inclination of stems, as the vegetation canopy height decreases so does the drag or the vegetative flow resistance (Kouwen and Li 1980; Tsujimoto et al.1996; Freeman et al. 2000). The vegetal resistance may reduce further to skin friction as highly bent flexible vegetation becomes a stream lined, thin layers similar to a smooth plate that exerts a minimum form drag on the flow (Li and Xi e2011).

A relationship between the deflected vegetation height and the flow drag exerted on vegetation elements is needed to iteratively determine the changing drag force and vegetation deformation. The study on submerged flexible plants by Kouwen and Unny (1973) expressed the deflected vegetation height as a function of the ratio of a stiffness parameter to the vegetal shear stress. Kouwen and Li (1980) reanalyzed the experimental data in Kouwen and Unny (1973) and proposed the deformation relation as seen in Eq.(9)

$$MEI_t = 0.25 \frac{H_v^2}{H_s} \quad (9)$$

For given parameters of EI, H_v , N, and t_v , H_s can be determined from one of the deformation relations defined by Eqs. (9)–(10). Upon knowing the deformation relation for a specific H_s :

where H_s is deflected vegetation stem height; MEI is stiffness parameter (EI) multiplied by the number of stems per square meter (M); t_v is vegetal stress, also known as the stress exerted on vegetation elements; E is modulus of elasticity ($N \times m^2$); and I is second moment of the cross section (m^4). Note that M is defined in the same way as the stem population density, N, except that M is effects of deformable plants on hydrodynamics, the treated as dimensionless. This equation is capped by $H_s = H_v$ when the plant rigidity is sufficiently larger than the imposed load. Substituting H^w for H^w in Eq.(6) and treating emergent and

plant type and a flow resistance law, one can determine the deflected vegetation height and the reduced vegetative flow resistance simultaneously by solving the two formulations iteratively.

A logarithmic formula of the flow resistance law was proposed by Kouwen and Unny (1973) and further examined by Kouwen and Li (1980) for submerged conditions.

$$\frac{1}{4} C_1 \log \frac{H_v}{C_0} \quad (11)$$

where f_s is friction factor including both the bed friction (f_b) and the vegetal friction (f_v); $f_s = f_v$ if the bed friction is omitted; C_0 and C_1 are empirical coefficients that may be obtained from regression of measurement data, which are dependent on vegetation properties and flow conditions.

Different coefficients were reported in previous studies

(e.g., Kouwen and Unny 1973; Carollo et al. 2005). Carollo et al. (2005) proposed another flow resistance formulation with more fitting coefficients involved under submerged conditions. To apply these formulations, laboratory experiments are desired to determine coefficients for the type of vegetation that is targeted in the field.

It has been demonstrated by Kutija and Hong (1996) that formulas developed for rigid vegetation could be extended to flexible ones by using the cantilever theory. The cantilever beam is defined as a pole with one end rigidly fixed to a support and the other end free to move. It is used to mimic the less rigid vegetation stem. The stem may be bent as the flow load increases; in return, the resistance

bending decreases. The balance position between the resistance

and the flow drag load is achieved dynamically and the solution can be found iteratively. To demonstrate the procedure and illustrate the

formulation proposed in Stone and Shen (2002) is adopted here because it employs less regression coefficients and it is valid for both submerged and emergent conditions. However, to apply the formulation, the wet vegetation height (H^w) needs to be replaced by the

deflected vegetation height (H^w). The descriptor w is mainly used for discriminating between emergent and submerged conditions; thus, H^w

for submerged conditions and $H^w = H_s$

for emergent conditions.

Using a different approach, Tsujimoto et al. (1996) applied finite

deformation theory of a cantilever beam and suggested a similar relation of the plant deformation as seen in Eq. (10)

$$\frac{H_s}{H_v} = \frac{NH^2EI}{141.020:89 \exp 24:66 t_v H^4} \quad (10)$$

where all symbols were defined in previous equations.

$f_v^{1/4}$

Fig.3. Sketch of flexible plant from erect to prone
 H_v vs

where s_c is critical value of submergence when $H_s = H_v$. Because of the deflection, plants get submerged before the water depth reaches the extent of the erect vegetation height. Therefore, the friction factor converges at a submergence smaller than 1 ($s_c < 1$). According to the hydraulic relationship between the friction factor and n , it is expected that n_c converges and reaches the maximum at s_c .

Experimental studies have shown that empirical formulations of n_c of deformable shrubs and woody vegetation for emergent and submerged conditions converge when the water depth is 80% of the erect vegetation height (Freeman et al. 2000; Copeland 2000). Taking Eq. (9) as an example of the deformation relation,

submerged conditions separately, a new relationship of the friction factor for flexible plants is expressed as

$$f_v^{1/4} = \frac{C_m N B H_s}{12 B_v N^2} \quad (12a)$$

$$s_c = \frac{H_v C_D N B_v H_v}{12} \frac{H_s^2}{H_v^2} \quad (12b)$$

$s_v N$

iteratively using Eqs. (9) and (12). A reduced friction factor is shown as the dashed curve in Fig. 2. The reduction becomes negligible when the degree of submergence is fairly large. For emergent conditions, the value of the friction factor overlaps with that of emergent rigid plants because no deflection formulation for emergent plants is considered. Note that both Eqs. (9) and (10) were deformation relations derived for submerged, flexible vegetation. Fathi-Maghadam and Kouwen (1997) and Kouwen and Fathi-Maghadam (2000) studied the deformation of cedar trees and demonstrated the reduction of the friction factor with increasing velocity; however, no convergence between the deflections of submerged plants and emergent plants has been found yet. Therefore, in this study, only the deflection of submerged vegetation is considered and emergent vegetation is assumed to act like rigid plants.

Numerical Implementation

The resistance force induced by vegetation has been included in the momentum equation as an extra term in many numerical studies (e.g., Lopez and Garcia 2001; Stoesser et al. 2003; Li and Yan 2007).

In the current study, the barotropic (horizontal 2D) model of an existing coastal ocean circulation model, ECOMSED (HydroQual 2002), is adopted, and a separate subroutine is developed to calculate the vegetalshear stress. The governing equations of the depth-integrated continuity equation and momentum equations with the extra term of vegetalshear stress are rewritten as

$$\frac{\partial h}{\partial t} + \frac{\partial v_x h}{\partial x} + \frac{\partial v_y h}{\partial y} = \frac{1}{4} F_{c,v} h^2 g h - \frac{1}{4} F_{d,f,x} \quad (13a)$$

where the number of iterations is usually less than 10.

The required input parameters for the vegetalshear stress module include H_v , B_v , EI , N , and C_D , (or C_0 , C_1 if the KL-extended approach is used).

only for submerged conditions. Therefore, during the transition from the submerged to emergent conditions, a linear interpolation is introduced for the continuity of the formulation and completeness of the approach. The KL-extended approach is applied for s_d (given sufficient submergence, e.g., $s_d \geq 1.5$), while the friction factor at s_c is computed using the SS-extended approach. In the transition zone ($s_c < s_d < 1.5$), the friction factor is obtained by linear interpolation.

Although different equations are implemented for deformable plants, the procedure of solving each set of equations is similar. Fig. 4 illustrates the iteration process using Eqs. (9) and (11) where Eq. (1) and the definition of the friction velocity $[V_p = 5 \tau_v / r^{0.5}]$ are introduced to rewrite those equations in terms of V_p and H_s , as Eqs. (14a) and (14b). The deflected vegetation height and the friction velocity are resolved iteratively.

Although different equations are implemented for deformable plants, the procedure of solving each set of equations is similar. Fig. 4 illustrates the iteration process using Eqs. (9) and (11) where Eq. (1) and the definition of the friction velocity $[V_p = 5 \tau_v / r^{0.5}]$ are introduced to rewrite those equations in terms of V_p and H_s , as Eqs. (14a) and (14b). The deflected vegetation height and the friction velocity are resolved iteratively.

$$H = \frac{MEI}{r} V_p^2 \quad (14a)$$

$$\frac{V_p}{2} = C_1 \log \frac{H_s}{C_0} \quad (14b)$$

In Fig. 4, the intersection of the two curves is the solution, while the circles connected by the thin, straight lines are quasi-solutions at iterative steps that gradually approach the final solution. The number

approach is used). The value of C_D for a single cylinder within a narrow channel is used. Other parameters are determined by laboratory or field

$$\frac{\partial v_x}{\partial t} + v_x \frac{\partial v_x}{\partial x} + v_y \frac{\partial v_x}{\partial y} = -\frac{1}{\rho} \frac{\partial p}{\partial x} + \nu \frac{\partial^2 v_x}{\partial x^2} + \nu \frac{\partial^2 v_x}{\partial y^2} + \frac{1}{\rho} \frac{\partial \tau_{yx}}{\partial y} - \frac{1}{\rho} \frac{\partial \tau_{xy}}{\partial x} + \frac{1}{\rho} F_{dif,x}$$

$$\frac{\partial v_y}{\partial t} + v_x \frac{\partial v_y}{\partial x} + v_y \frac{\partial v_y}{\partial y} = -\frac{1}{\rho} \frac{\partial p}{\partial y} + \nu \frac{\partial^2 v_y}{\partial x^2} + \nu \frac{\partial^2 v_y}{\partial y^2} + \frac{1}{\rho} \frac{\partial \tau_{yx}}{\partial y} - \frac{1}{\rho} \frac{\partial \tau_{xy}}{\partial x} + \frac{1}{\rho} F_{dif,y}$$

$$\frac{\partial h}{\partial t} + v_x \frac{\partial h}{\partial x} + v_y \frac{\partial h}{\partial y} = \frac{1}{\rho} \frac{\partial \tau_{yx}}{\partial y} - \frac{1}{\rho} \frac{\partial \tau_{xy}}{\partial x} + \frac{1}{\rho} F_{dif,y} - \frac{1}{\rho} F_{dif,x}$$

(13c)

measurements of the vegetation. The numerical model incorporating the vegetation module is tested against three laboratory measurements. Specific boundary

conditions are given in accordance with the laboratory experimental setup.

Model Testing

where t is time; h is water surface elevation above the still water datum; v_x and v_y are depth-averaged velocities in the x - and y -directions, respectively; h is total water depth; F_c is Coriolis force coefficient; g is acceleration due to gravity; $F_{dif,x}$ and $F_{dif,y}$ are the horizontal diffusion terms in the x - and y -directions, respectively; τ_0 , τ_b , and τ_v are wind stress, bottom shear stress, and the vegetal shear stress, respectively; and their subscripts represent the components in the x - and y -directions. The vegetal shear stress is calculated in a separate module using the methodology and algorithm described in the previous section. It is then passed to the momentum equations at each time step where the velocity components and surface elevation are resolved. Three approaches are implemented to account for rigid plants, unyieldingly deformable plants, and yieldingly deformable plants.

In Approach 1, Eq. (6) is utilized to calculate the friction factor for rigid plants. In Approach 2, Eq. (12) extended from the formula for rigid vegetation and Eq. (9), the plant deformation relationships are employed for deformable plants with a certain degree of rigidity. This procedure is valid for a wide range of submergence, hereafter known as the SS-extended (Stone and Shen extended) approach. In Approach 3, Eq. (11) developed for highly flexible plants and the plant deformation relationships of Eq. (9) are employed for flexible plants, hereafter known as the KL-extended (Kouwen and Li extended) approach. Because Eq. (11) was developed from

Emergent Vegetation

Tsujimoto and Kitamura (1995) designed a flume that mimics a compound channel by covering the bed partially with emergent

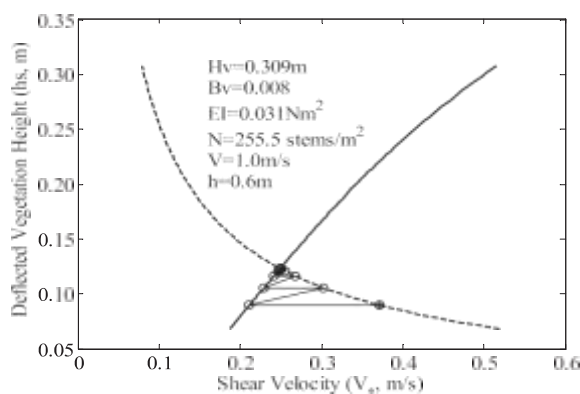


Fig.4. Iterative solution of shear velocity and deflected vegetation height for flexible plants [dashed line, using Eq. (14a); th

using Eq. (14b); thin line with circles, iteration steps]

ments of submerged vegetation, the KL-extended approach is valid for cylindrical rods (bamboo, vinyl chloride, and nylon). Quasi-uniform flows over the channel were studied through five sets of experiments (A through E), among which there were three experimental data sets (A1, B1, and C1) presented in Tsujimoto and Kitamura (1995). In this study, only the data sets from experiments with bamboo are utilized, that is, A1 and B1. The flume was 12 m long and 0.4 m wide with emergent bamboo covering a 0.12-m-wide vegetation zone (Fig. 5). Bamboo plants with a diameter of 0.15 cm were distributed in a parallel pattern and the spacing of vegetation elements was 2.8 cm for A1 and 2.0 cm for B1. For both experiments, the channel bed slope was $1:73 \times 10^{-3}$. The mean channel-average flow velocity, the mean flow depth, and the friction factor in the main course were given as control parameters of the experiments. The cross-sectional average velocity was measured 40 cm downstream using a series of electromagnetic anemometers. The stem density and the drag coefficient (C_D) as two of the

vegetation-property input parameters are calculated according to the information provided in Tsujimoto and Kitamura (1995) and listed in Table 2. Approach 1 for rigid plants is used in this test. The drag coefficient C_D input to the model is related to the bulk drag coefficient (C_D) for the emergent condition using Eq. (5a), where C_D is computed using the given values of the friction coefficient ($V^2 = 2C_D B_v N h$) over the vegetation bank in Tsujimoto and Kitamura (1995). The value of the friction coefficient (C_f) for the main course of the channel was given in Tsujimoto and Kitamura (1995) and used to calculate $t_b = 5rC_f V^2$. The model domain covers the entire flume range with $\Delta x = 5.2$ cm, $\Delta y = 2$ cm, and $\Delta t = 0.005$ s. It takes 218 s to reach a steady state when model results are output and compared with experimental data. The bottom panel in Fig. 5 shows good agreement between the modeled and experimental results. The numerical model shows that the bamboo field considerably reduces the flow velocity in the vegetation zone, consistent with the measurements. The light

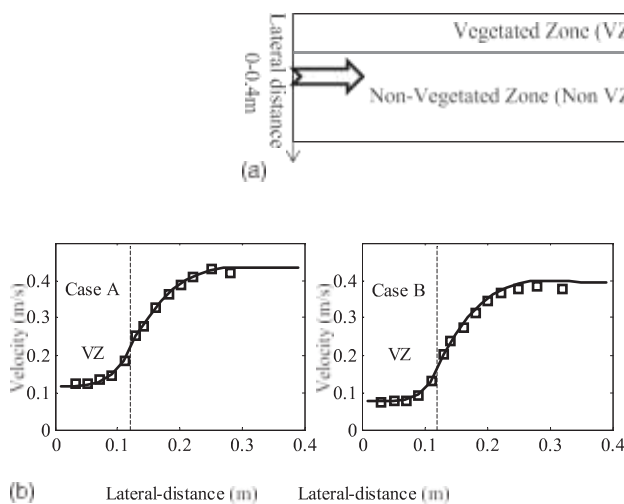


Fig.5.(a) Plan view of the experiment setup adapted from Tsujimoto and Kitamura (1995); (b) comparison of measured (squares) and modeled (solid lines) depth-averaged velocities

overestimate of velocity in the main course of the channel is caused by the lack of wall friction in the numerical model. In the vegetation zone, the agreement is better as the effect of the wall friction is negligible compared with the flow resistance due to the bamboo.

Submerged Rigid Vegetation

Lopez and Garcia (1997) conducted a series of

laboratory experiments under uniform flow conditions in a 19.5-m-long, 0.91-m-wide, and 0.61-m-deep tilting flume. The first approach for rigid vegetation implemented in the storm surge model is applied and tested against the experiments with submerged rigid cylinders (#1 through #12). Table 3 lists the experimental conditions and model results. The drag coefficient, C_D , is set to 1.05 according to

Stone and Shen (2002). The stem density, N , is computed using the stem diameter ($B_s = 0.64$ cm) and the plant population density ($a = 5 N 3 B_s$) provided in Lopez and Garcia (1997). An average value of bed friction coefficient is estimated following the procedure introduced in Stone and Shen (2002) (see Appendix) because no bottom friction parameters were provided in Lopez and Garcia (1997). The open channel flow is modeled using a grid with resolution of $dx = 20$ cm and $dy = 15$ cm. The time step is set to $dt = 0.01$ s and the steady state is reached after 73 s.

The model results agree well with the laboratory measurements.

The square of correlation coefficient (R^2) for the average depth, depth-averaged velocity and average surface slope against laboratory measurements are 0.994, 0.995, and 0.995, respectively, as shown in Table 3. The RMS error for each output parameter is also listed in Table 3.

Submerged Flexible Vegetation

Flow resistance of a deformable vegetation field is different from that of rigid plants, as the deformable plants are bent by the drag force of the flow. In return, the bent plants reduce the vegetation-induced resistance to the flow. A

dynamic balance exists between the deflected vegetation and the flow. Järvelä (2005) conducted flume studies and provided a dataset of mean velocity of flow over flexible vegetation. The flume was 50 m long and 1.1 m wide. Natural wheat ($H_s = 28$ cm and $B_s = 2.8$ cm) was planted in the flume with an average density of $12,000$ stems $= m^{-2}$ and covered a 6-m-wide zone in the middle of the flume. An adjustable overflow weir was used to achieve desired water depth. Four flow depths were used and total nine tests were carried out with three discharges. The deformation relation, Eq. (9), was adopted to calculate the flexibility, $MEI = 1.2 N \times m^2$. For detailed information about the laboratory experiment, the reader is referred to Järvelä (2005).

By applying the KL-extended approach that solves Eqs. (9) and (11) iteratively, the vegetal stress and the deflected vegetation height were obtained. Note that two coefficients (C_0 and C_1) are required by this method in the logarithmic formulation of a flow resistance law, which need to be calibrated for the different types of vegetation (Kouwen and Li 1980; Kouwen 1992; Carollo et al. 2005).

Table 2. Input Parameters for Numerical Simulations with Emergent Vegetation

Tests	Flow depth (cm)	Cross section average velocity (cm/s)	Channel friction coefficient (3×10^{-3})	Element spacing (m)	Stem density (number $= m^{-2}$)	Vegetation bank friction coefficient	Characteristic drag coefficient
	h	V	C_f	d	N	V	C_D
Case A	4.57	32.0	3.8	0.028	1,275.5	0.050	1.054
Case B	4.28	27.6	4.0	0.020	2,500.0	0.116	1.239

Laboratory or field experiments are desirable for determining the vegetation specific coefficients of C_0 and C_1 .

In the numerical simulation, $C_0 (0.494)$ and $C_1 (7.315)$ were

predetermined by fitting the experimental data to the logarithmic formula, Eq. (11), with $R^2 = 0.92$. The numerical model was set up according to the laboratory conditions and the downstream water surface level is adjusted to achieve the measured flow depths with RMS error 5.5×10^{-25} m. All simulations use the same mesh with $dx = 20$ cm, $dy = 15$ cm, and run with $dt = 0.01$ s. Slightly different time spans are required to reach the steady state for various cases, ranging from 548 to 903 s. Table 4 lists the laboratory data (discharge, flow depth, water surface slope, and deflected plant height) and model results. Good agreement is seen for cases of large

relative submergence, whereas underestimation of the surface slope occurs for cases of small relative submergence (#1 and #2). This suggests that the KL-extended method is valid for a large submergence but gives large error for near-emergent cases.

The SS-extended method is not applied to this test case because no drag coefficient was provided in Järvelä (2005) and the C_D of

1.05 used previously may not be applicable for the experimental material (wheat seedlings) of a fairly flexible form, and further-more, the experimental plants field of a fairly large stem density, $N = 12,000 = m^{-2}$.

II. SUMMARY AND CONCLUSIONS

The paper has extended and unified resistance formulations for rigid, flexural rigid, and flexible plants under both emergent and sub-

merged conditions. Three approaches were examined in detail and implemented into a storm surge model. First, the flow resistance formulations for rigid plants were critically reviewed. By introducing the plant deformation relations, the formulation for rigid plants developed by Stone and Shen (2002) was extended to flexural rigid (or unyieldingly flexible) plants, namely the SS-extended approach, in which the deflected vegetation height substitutes the erect height of rigid vegetation. Both the rigid formulation and the SS-extended approach are valid continuously for a wide range of submergence from emergent to submerged conditions. The formula for rigid plants was tested against laboratory measurements while the

SS-extended approach was only checked analytically owing to the lack of observation data for unyieldingly flexible plants. As the plant stiffness parameter becomes sufficiently large, the solution converges to that of the rigid formula. In Fig. 2, the friction factor for deformable plants (dashed line) predicted by the SS-extended will shift upward and approach the solution of rigid plants (solid line) for large plant rigidity. Another flow resistance formulation directly derived from submerged, yieldingly flexible plants by Kouwen and Li (1980) was

Table 3. Laboratory Measurements and Numerical Model Results of Uniform Open-Channel Flow over Rigid Plants

number	(a_1 , m^2)	$h(m)$	$Q(m^3/s)$	$V(m/s)$	Averaged surface slope	$h(m)$	$V(m/s)$	Averaged surface slope
1	1.09	0.335	0.179	0.587	0.0036	0.334	0.589	0.0035
2	1.09	0.229	0.088	0.422	0.0036	0.230	0.421	0.0036
3	1.09	0.164	0.046	0.308	0.0036	0.165	0.306	0.0037
4	1.09	0.276	0.178	0.709	0.0076	0.274	0.715	0.0075
5	1.09	0.203	0.098	0.531	0.0076	0.202	0.534	0.0075
6	0.27	0.267	0.178	0.733	0.0036	0.262	0.746	0.0032
7	0.27	0.183	0.095	0.570	0.0036	0.182	0.575	0.0035
8	2.46	0.391	0.180	0.506	0.0036	0.393	0.503	0.0038
9	2.46	0.214	0.058	0.298	0.0036	0.220	0.289	0.0041
10	2.46	0.265	0.180	0.746	0.0160	0.273	0.723	0.0163
11	0.62	0.311	0.177	0.625	0.0036	0.305	0.638	0.0031
12	0.62	0.233	0.181	0.854	0.0110	0.223	0.894	0.0107
					R^2	0.994	0.995	0.995
					RMS error	0.0050	0.0149	0.00027
					Percent error	1.95%	2.60%	4.56%

Experiment

Plant density

Experimental conditions Model results

Table 4. Model Setup and Model Results

Experiment number	Discharge (m^3/s)	Depth (m)	Deflected vegetation surface slope (%)	Deflected vegetation height (m)	Deflected vegetation surface slope (%)	Deflected vegetation height (m)
1	0.040	0.3060	0.15	0.205	0.12	0.191
2	0.100	0.3084	0.36	0.155	0.32	0.132

3	0.040	0.4065	0.05	0.230	0.05	0.248
4	0.100	0.4041	0.13	0.190	0.13	0.169
5	0.143	0.4070	0.20	0.160	0.19	0.145
6	0.040	0.5044	0.02	0.245	0.02	0.280
7	0.100	0.4950	0.06	0.220	0.06	0.204
8	0.100	0.7065	0.02	0.260	0.02	0.279
9	0.143	0.7037	0.03	0.215	0.03	0.235
				R ²	0.993	0.937
RMSerror					0.017	0.0210
Percenterror					15.00%	10.05%

also examined and extended, namely, the KL-extended approach. This approach essentially covers only submerged conditions. However, to avoid discontinuity and numerical instability, near emergent

• Step 7. Convert f_b to the bed friction coefficient C_f as in the quadratic law ($\tau = C_f V^2$) by invoking Eqs. (16) and (17)

to fully submerged conditions were considered using the linear interpolation in the transition zone. The degree of full submergence

(s_d) is recommended to be 1.5 according to Nepf and Vivoni (2000), $C_f^{1/4}$ $f_b^{1/2} \frac{1}{h^2}$

$$12B^P N^2$$

$$p_{iii_2} \quad (18)$$

above which a logarithmic nonvegetation flow starts developing beyond the mixing layer. Both the KL-extended and SS-extended approaches solve a set of two equations, that is, a deformation relation and a resistance law, iteratively, in a similar fashion. The three approaches have been implemented into a storm surge model as three options. Good agreement with laboratory measurements has been found for the approach of rigid plants and the KL-extended approach. The SS-extended approach analytically tested is promising because it accounts for both the flexibility of natural plants and a full range of submergence. However, further tests against observations are desirable for future research. In summary, this study has developed a physics-based procedure to incorporate the effects of deformable vegetation into a numerical storm surge model and unified formulations for emergent, near-emergent, and fully submerged rigid or flexible vegetation. A sub-model of vegetal stress and deflected vegetation height was

developed and tested against laboratory experiments. To improve the prediction of surge reduction by wetland vegetation, quantifying the spatial and temporal variations of deflected vegetation heights and equivalent Manning's coefficient under realistic field conditions is of significance and will be discussed in an upcoming paper.

Appendix. Estimate of Bed Friction Coefficient

The flow depth, depth-averaged velocity, and bed slope are available in the experimental data sets. The bed friction factor is estimated by using the method provided in Stone and Shen (2002).

- Step 1. Initiate the channel bed friction factor f_b
- Step 2. Calculate C_f using

The average value of C_f is estimated to be 0.0072 $\frac{h^p}{N}$

REFERENCES $12B, h^p N$

- [1]. Alongi, D.M. (2008). "Mangrove forest: Resilience, protection from tsunamis, responses to global climate change." *Estuar. Coast. Shelf Sci.*, 76(1), 1–13.
- [2]. Arcement, G.J.J., and Schneider, V.R. (1989). "Guide for selecting Manning's roughness coefficients for natural channels and floodplains." U.S. Geological Survey Water-Supply Paper No. 2339, U.S. Dept. of the Interior, USGS, Reston, VA.
- [3]. Barkdoll, B. D., Vittilam, S., Bennett, S. J., and Alonso, C. V. (2004). "Flow resistance of emergent vegetation." *Proc., World Water and Environmental Resources Congress 2004 (CD-ROM)*, G. Sehlke, D.F. Hayes, and D. K. Stevens, eds., ASCE, Reston, VA.
- [4]. Bunya, S., et al. (2010). "A high-resolution coupled riverine flow, tide, wind, wind waves, and storm surge model for southern Louisiana and Mississippi. Part I: Model development and validation." *Mon. Weather Rev.*, 138(2), 345–377.
- [6]. Carollo, F. G., Ferro, V., and Termini, D. (2005). "Flow resistance law

- in channels with flexible submerged vegetation.
” J. Hydraul. Eng., 10.1061/(ASCE)0733-9429(2005)131:7(554),554–564.
- [7]. Chen, Q., Wang, L., and Tawes, R. (2008). “Hydrodynamic response of northeastern Gulf of Mexico to hurricanes.” *Estuaries Coasts*, 31(6), 1098–1116.
- [8]. Chen, Q., and Zhao, H. (2012). “Theoretical models for wave energy dissipation caused by vegetation.” *J. Eng. Mech.*, 10.1061/(ASCE)EM.1943-7889.0000318, 221–229.
- [9]. Chow, V. T. (1959). *Open-channel hydraulics*, McGraw Hill, New York.
- Costanza, R. R. (2000). “Determination of flow resistance coefficients due to shrubs and woody vegetation.” *CHETN-VIII-3*, U.S. Army COE, Washington, DC.
- [10]. Costanza, R., Pérez-Maqueo, O., Martínez, M. L., Sutton, P., Anderson, S. J., and Mulder, K. (2008). “The value of coastal wetlands for hurricane protection.” *Ambio*, 37(4), 241–248.
- [11]. Day, J. W. J., et al. (2007). “Restoration of the Mississippi Delta: Lessons from Hurricanes Katrina and Rita.” *Science*, 315(5819), 1679–1684.
- [12]. Day, J. W. J., et al. (2007). “Restoration of the Mississippi Delta: Lessons from Hurricanes Katrina and Rita.” *Science*, 315(5819), 1679–1684.